Plasmonic Rainbow Trapping Structures for Light Localization and Spectrum Splitting

Min Seok Jang and Harry Atwater

Phys. Rev. Lett. **107**, 207401 — Published 8 November 2011

DOI: 10.1103/PhysRevLett.107.207401

Plasmonic Rainbow Trapping Structures for Light Localization and Spectrum Splitting

Min Seok Jang and Harry Atwater

Thomas J. Watson Laboratories of Applied Physics,

California Institute of Technology, MC 128-95, Pasadena, CA 91125

Abstract

"Rainbow trapping" has been proposed as a scheme for localized storage of broadband electromagnetic radiation in metamaterials and plasmonic heterostructures. Here, we articulate the dispersion and power flow characteristics of rainbow trapping structures, and show that tapered waveguide structures composed of dielectric core and metal cladding are best suited for light trapping. A metal/insulator/metal taper acts as a cascade of optical cavities with different resonant frequencies, exhibiting a large quality factor and small effective volume comparable to conventional plasmonic resonators.

Body

Slow electromagnetic waves, first studied in systems with atomic coherence at low temperature [1], have been investigated in recent years at room temperature via light dispersion in solid state media such as photonic crystals [2, 3]. However most of these systems operate only at specific resonant frequencies, and so broadband light trapping remains a great challenge. Tsakmakidis et al. first proposed "rainbow trapping" in which a wide wavelength range of electromagnetic fields can be trapped in tapered waveguide structures composed of negative index core and dielectric cladding (insulator-negative index-insulator, or INI) which exhibits a negative Goos-Hänchen effect [4]. Recently, researchers have determined that such trapping mechanism is also applicable for transverse magnetic

(TM) waves in insulator-metal-insulator (IMI) and metal-insulator-metal (MIM) waveguide tapers under certain material property conditions [5, 6]. However, to date the question of how much light a rainbow trapping structure can actually store and how the light escapes from it has not been addressed.

In this work, we study fundamental mode conversion and loss mechanisms of linearly-tapered INI, IMI and MIM rainbow trapping structures and show that MIM rainbow trapping structures are superior to the others in terms of trapping performance. Assuming a Drude dispersion relation for the cladding metal, we specify the frequency range and the structural dimensions needed to achieve rainbow trapping and calculate the quality factor Q and the effective mode area A_{eff} as quantitative measures of light trapping and localization. We perform a transfer matrix analysis [7] to examine the behavior of the guided modes in the structure, and confirm the results with full-wave finite difference time domain (FDTD) and finite element method (FEM) simulations. The paper is organized as follows: Figure 1 illustrates the mode conversion properties of IMI, INI and MIM tapers. We then compare the energy density distributions and modal amplitudes achievable for IMI TM_0 modes and MIM TM_2 modes, as indicated in Fig. 2. For MIM tapers, we then investigate the critical taper thickness for mode conversion and the quality factor achievable for the quasi-bound mode as a function of frequency. Finally we explore the properties of rainbow tapers as a function of taper angle, as illustrated by Fig. 4.

The dispersion relations of eigenmodes in rainbow trapping systems are exotic. Figure 1(d), (e) and (f) respectively show the effective indices n_{eff} of IMI TM_0 modes and TM_2 modes in INI and MIM tapers as a function of core thickness α. For all three cases, the modes consist of two branches; the energy velocity, $v_E = \int S_z dx / \int u dx$, where u and $\mathbf{S}$ are the time averaged energy density [8] and Poynting vector, and the phase velocity are parallel for one branch ($|f\rangle$) and antiparallel for the other ($|b\rangle$), as seen in Fig. 1(g)-(i). Since each mode can propagate along either the $+z$ or $-z$ direction, there

exist a total of four orthogonal eigenmodes $|f+\rangle$, $|f-\rangle$, $|b+\rangle$ and $|b-\rangle$. The letters f and b identify the branch and the signs $+$ and $-$ indicate the direction of energy propagation. If the system is adiabatic enough to neglect the coupling between these modes and higher order modes, it is possible to describe the system as a linear superposition of these four basis modes. The $|f\rangle$ and $|b\rangle$ are degenerate at a certain core thickness, α_d, and the dispersion relations splits as α deviates from α_d. It is worth noting that the direction of power flow through the cladding is opposite to the flow through the core and their magnitudes become equal at $\alpha = \alpha_d$ which results in zero energy velocity. The conditions for having degeneracy points are specified in Table 1[5, 6].

Many simulation results have shown that it is impossible to trap light to a complete standstill even under the assumption of lossless materials [5, 9, 10]. This results from the coupling between the eigenmodes due to the fundamental nonadiabaticity near $\alpha = \alpha_d$. More specifically, the slow core thickness variation condition [11], $d\alpha / dz \ll \alpha k_0 \Delta n / \pi$, where k_0 is the wavenumber in the free space and Δn is the effective index difference between eigenmodes, can never be fulfilled throughout the entire structure because $\Delta n = 0$ at the degeneracy point. In fact, the degeneracy point connects $|f\pm\rangle$ to $|b\mp\rangle$. Mechanisms for power flow into and out of rainbow trapping structures are schematically described in Fig. 1(a)-(c). An incident IMI TM_0 $|f+\rangle$ is converted to the other branch $|b-\rangle$ at $\alpha = \alpha_d$ and escapes the structure. In an INI structure, an incident photonic $|b+\rangle$ is converted to $|f-\rangle$ at $\alpha = \alpha_d$ and couples into a backward propagating radiative mode at $\alpha = \alpha_r$, where n_{eff} coincides with the index of the cladding. An incident MIM photonic $|f+\rangle$ undergoes similar mode conversion at the degeneracy point but the converted $|b-\rangle$ is reflected to $|b+\rangle$ at the mode cutoff $\alpha = \alpha_c$, and converted back to $|f-\rangle$, which finally escapes the structure. The reflection at $\alpha = \alpha_c$, where the energy velocity also

vanishes, makes electromagnetic waves reside longer in the taper segment between the degeneracy point and the mode cutoff.

One can intuitively sketch out the mode conversion mechanism in an analogous ray optic picture. A light ray incident upon a core/cladding interface at an angle of incidence Θ_0 undergoes total internal reflection with negative Goos-Hänchen shift, propagates in the core, and strikes the other interface with angle $\Theta_0 - \theta$, where θ is the taper angle. Since the successive angle of incidence $\Theta_N = \Theta_0 - N\theta$ decreases as the number of bounces N increases, the lateral propagation of the ray between two consecutive Goos-Hänchen shifted internal reflections also decreases, crosses zero, and becomes negative which corresponds to our mode conversion description at $\alpha = \alpha_d$. For INI structures, the light ray escapes the structure in the form of radiation once Θ_N reaches the angle of escape Θ_r determined by Snell's law (Fig. 1(b)). Therefore a ray can bounce M times, where M is the largest integer satisfying $\Theta_M > \Theta_r$ (i.e. $M \sim (\Theta_0 - \Theta_r)/\theta$). On the other hand, in MIM structures, the light ray is always totally reflected at the interface. Therefore Θ_N can be further reduced and cross zero at the mode cutoff ($\alpha = \alpha_c$) (Fig. 1(c)). From there, the ray travels back in the $+z$ direction again and then repeats the same process that we described previously but in the reverse manner. The number of internal reflections is thus $M \sim 2\Theta_0/\theta$, which is greater than that of the INI case.

We perform a transfer matrix analysis to quantitatively understand the behavior of the modes in the IMI and MIM rainbow trapping structure by computing the amplitude of the eigenmodes. The mode amplitudes are normalized such that $|a|^2 = \left| \int dx (\mathbf{E} \times \mathbf{H})_z / 2 \right|$, where $\mathbf{E}$ and $\mathbf{H}$ are electric and magnetic fields of the corresponding mode. Note that, for modes having real propagation constants, $|a|^2$ is simply the time-averaged power flow. Fig. 2(c) shows the mode amplitudes of IMI TM_0 modes in the steady

state. Corresponding to our previous description, a_{f+} and a_{b-} are of similar magnitude whereas a_{f-} and a_{b+} are very small, which indicates mode conversion from $|f+\rangle$ to $|b-\rangle$, with other modes suppressed. On the other hand, for MIM TM_2 mode trapping, $|a_{f+}| \sim |a_{f-}|$ where $\alpha > \alpha_c$ and $|b+\rangle$ and $|b-\rangle$ are excited only in the taper section $\alpha \in (\alpha_d, \alpha_c)$ and decay as they become evanescent (Fig. 2(d)). Due to the simultaneous excitation of $|f+\rangle$, $|f-\rangle$, $|b+\rangle$ and $|b-\rangle$, an MIM structure can store large amounts of energy which makes them the best candidates for trapping light. Although an IMI structure can perform as a compact mode converter, its light trapping capability is inferior to the MIM trapping structure because it does not exhibit mode cutoff (Fig. 2(a) and (b)). Due to the inevitable radiation loss, in addition to the difficulties in fabrication, INI rainbow trapping seems less attractive compared to the other approaches. Therefore, we focus our attention on MIM rainbow trapping in the rest of the discussion.

Although rainbow trapping structures are open systems, they can be considered as a series of optical cavities having different resonant frequencies since they can localize broadband light in tapered sections of different width depending on frequency. Assuming a dispersionless dielectric core and a Drude metal cladding of $\varepsilon_{\mathrm{II}}(\omega) = 1 - \omega_p^2 / (\omega^2 + i\Gamma\omega)$ where ω_p and Γ are the plasma frequency and the damping constant respectively, TM_2 modes at frequency $\omega / \omega_p \in \left((0.2430\varepsilon_{\mathrm{I}} + 1)^{-1/2}, 1\right)$ can be trapped in the structure (Table 1). We plot α_d, α_c and n_d as functions of ω in Fig. 3(b). As a measure of trapping performance, we calculate the quality factor Q from electric and magnetic field distribution in the steady state. Q is defined by $\omega U / P$ where P is the power dissipated and U is the energy stored in the rainbow trapping structure ($z > 0$) having the entrance thickness α_0 (see inset of Fig. 3(a)). Here, α_0 is chosen to be $\max\{\alpha_c(\omega)\}$ to ensure the structure to be functional for the entire target frequency range.

Recognizing that the input power is equal to the dissipated power in steady state, and that the only incoming guided mode at the entrance ($z = 0$) is $|f+\rangle$, P is equal to the incoming power carried by $|f+\rangle$. Since the wave propagates deeper along the taper, Q increases as ω increases for a fixed taper angle $\theta = 2^\circ$ (Fig. 3(d)). It is worth noting that Q is directly proportional to the light trapping time $\tau = Q/\omega$. For instance, for $\theta = 2^\circ$ and $\omega/\omega_p = 0.6$, τ is calculated to be around 33 periods which is quite a long time since the distance between the entrance and the degeneracy point is only about 1.5 effective wavelengths. We confirm that τ corresponds to the actual signal trapping time by measuring the time it takes by a pulse to escape a rainbow trapping structure by FDTD simulations. Interestingly, the signal trapping time does not vary significantly from the value of the lossless case but only causes the outgoing signal to attenuate as Γ becomes larger.

When material loss is present ($\Gamma \neq 0$), the degeneracy between $|f\rangle$ and $|b\rangle$ is removed and v_E thus has finite value everywhere (Fig. 1(f)). However, the overall power flow and optical dispersion characteristics – v_E drops down significantly and that the effective indices of $|f\rangle$ and $|b\rangle$ get very close to each other around $\alpha = \alpha_d$ – are preserved. Thus the previously described light trapping mechanism is still valid except at very high loss. For a fixed frequency, Q is found to be almost inversely proportional to the taper angle. As $\theta \to 0$, Q becomes limited by ohmic loss inside the metal alone, asymptotically approaching $c/2v_E \,\mathrm{Im}\{n_{\mathrm{eff}}^{f+}(\alpha = \alpha_0)\}$ (Fig. 4(b)).

We also calculate the effective area A_{eff} for our two-dimensional rainbow trapping structure as a measure of light localization, $A_{\mathrm{eff}} = U / \max\{u(x,z)\}$, where (x,z) reside in the dielectric core where an object may be placed to interact with the field. By conservatively assuming a diffraction-limited height $L_y = \lambda_0 / 2n_{\mathrm{I}}$, the effective volume can be approximated as $V_{\mathrm{eff}} \sim A_{\mathrm{eff}} \lambda_0 / 2n_{\mathrm{I}}$. Fig. 4(d) displays Q/V_{eff}

of TM_2 modes as a function of inverse angle θ^{-1}. When $\Gamma = 0$, Q/V_{eff} monotonically increases since adiabatic condition holds up to α closer to α_d as θ gets smaller. In the presence of material loss, the effect of rainbow trapping and propagation losses compete. The Q/V_{eff} is dominated by propagation loss for very small taper angle whereas the rainbow trapping effect dominates it for relatively large θ, because propagation loss exponentially increases as a function of propagation distance. Therefore Q/V_{eff} has a maximum where both effects are balanced. For greater values of Γ, the optimal θ increases to compensate higher propagation loss.

We note that TM_1 modes at $\omega/\omega_p \in \left((1.3510\varepsilon_I+1)^{-1/2},(\varepsilon_I+1)^{-1/2}\right)$ can also be trapped in the MIM taper structures. The parameters α_d and α_r of TM_1 modes have similar order of magnitude to those TM_2 modes, implying that both type of modes can be trapped in a single structure (Fig. 3(a)). However, unlike TM_2 or higher order photonic modes, TM_1 modes are mostly anti-symmetric superpositions of surface plasmon polariton modes. Their field intensity is greatest at the metal/dielectric interfaces and exponentially decays as a function of distance from the interface, making them slow compared to the photonic modes and very sensitive to changes at the vicinity of the surface. Due to the small energy velocity, Q of TM_1 modes tends to be much higher than that of photonic modes and even diverges when ω approaches to surface plasmon resonance frequency if the metals are lossless (Fig. 3(c)). Moreover, since the energy of TM_1 modes is highly confined at the interfaces, they can have very small A_{eff} well below the diffraction limit (Fig. 4(c)). However, because of the significant energy penetration into the metal, TM_1 modes are much sensitive to the material loss than TM_2 modes, making it difficult for them to exhibit a rainbow trapping effect for the realistic damping constant $\Gamma/\omega_p \sim 0.01$ [12].They also undergo non-negligible reflection due to the tapering. This adds distinctive Fabry-Perot

type oscillations as a function of the taper length, as illustrated in Fig. 4(a) and (c). The TM_1 modes might not be suitable for signal processing since the shape of a signal can be significantly distorted by this reflection.

In order to exhibit rainbow trapping effect for a wide range of frequencies, dielectric core materials should have sufficiently high index and the metal cladding should have low ohmic loss and simultaneously satisfy the conditions specified in Table 1. In the optical frequency range, MIM rainbow tapers with Ag [12] as the metallic layer and GaP [13] as the dielectric are able to trap TM_1 modes for wavelengths ranging from 540 to 590 nm at α of 22-48 nm. For a Ag/GaP/Ag taper of $\alpha_0 = 50\,\text{nm}$ and $\theta = 5^\circ$, we obtain Q~30-60 and $A_{\text{eff}}(\lambda_0 / n_1)^{-2}$~0.01-0.1 throughout the target wavelength range (see Supplementary Information). One could also trap infrared light by utilizing polar dispersive materials that support phonon-polariton modes as negative permittivity claddings. For instance, SiC/Si/SiC heterostructures are able to localize TM_2 modes in infrared regime near the SiC phonon polariton resonance (~10.5 μm) where the permittivity of SiC varies from positive to negative with very small damping [14].

In summary, rainbow trapping structures composed of insulating core and metal claddings offer better trapping performance compared to INI or IMI structures. We have also shown that MIM rainbow trapping structures can exhibit large broadband Q and Q / V_{eff} comparable to those of existing plasmonic cavities [15, 16]. It should also be possible to reduce the propagation loss by configuring the taper profile of rainbow trapping structures to be other than linear. Rainbow trapping structures may also find application as materials that surpass the classical light trapping limit [17] and which enhance the efficiency of solar cells by trapping different frequency bands of the solar spectrum into semiconductors of different band gaps arrayed along the taper in order to maximize the solar absorption.

Further investigations may also lead to applications in optical signal processing by utilizing the electro-optic effect.

We thank Stanley Burgos and Eyal Feigenbaum for helpful comments. This work was supported by the Light-Material Interactions in Energy Conversion Center, an Energy Frontier Research Center of the Office of Science of the Department of Energy under grant DE-SC0001293.

References

1. C. Liu, Z. Dutton, C. H. Behroozi, and L. V. Hau, Nature (London) **409**, 490 (2001).
2. H. Gersen, T. J. Karle, R. J. P. Engelen, W. Bogaerts, J. P. Korterik, N. F. van Hulst, T. F. Krauss, and L. Kuipers, Phys. Rev Lett. **94**, 073903 (2005).
3. Y. A. Vlasov, M. O'Boyle, H. F. Hamann and S. J. McNab, Nature **438**, 65 (2005).
4. K. L. Tsakmakidis, A. D. Boardman, and O. Hess, Nature (London) **450**, 397 (2007).
5. W. T. Lu, Y. J. Huang, B. D. F. Casse, R. K. Banyal, and S. Sridhar, Appl. Phys. Lett. **96**, 211112 (2010).
6. J. Park, K. Y. Kim, I. M. Lee, H. Na, S. Y. Lee, and B. Lee, Opt. Express **18**, 598 (2010).
7. A. Yariv, IEEE J. Quantum Electron. **QE-9**, 919 (1973).
8. R. Ruppin, Phys. Lett. A **299**, 3092 (2002).
9. J. He, Y. Jin, Z. Hong and S. He, Opt. Express **16**, 11077 (2008).
10. T. Jiang, J. Zhao and Y. Feng, Opt. Express **17**, 170 (2009).
11. A. Snyder and J. D. Love, *Optical Waveguide Theory* (Chapman and Hall, New York, 1983).
12. P. B. Johnson and R. W. Christy, Phys. Rev. B **6**, 4370 (1972).
13. E. D. Palik, *Handbook of Optical Constants of Solids* (Academic, 1985).
14. W. G. Spitzer, D. A. Kleinman, and D. Walsh, Phys. Rev. **113**, 127 (1959).

15. H. T. Miyazaki, Y. Kurokawa, Phys. Rev. Lett. **96**, 097401 (2006).

16. B. Min, E. Ostby, V. Sorger, E. U. Avila, L. Yang, X. Zhang, and K. Vahala, Nature (London) **457**, 455 (2009).

17. E. Yablonovitch and G. D. Cody, IEEE Trans. Electron Devices **29**, 300 (1982).

Tables and Figures

INI, NIN	MIM	IMI
$\mathrm{TM}_0 : \sigma_\varepsilon > \max\{1, \sigma_\mu^{-1}\}$ $\mathrm{TM}_1 : 1 < \sigma_\varepsilon < \sigma_\mu^{-1}$ $\mathrm{TM}_{m\geq 2} : \sigma_\varepsilon \sigma_\mu < 1$	$\mathrm{TM}_1 : 1 < \sigma_\varepsilon < 1.3510$ $\mathrm{TM}_{m\geq 2} : \sigma_\varepsilon^{-1/2} + \mathrm{atan}\left(\sigma_\varepsilon^{-1/2}\right) > \frac{m\pi}{2}$	$\mathrm{TM}_0 :$ $\sigma_\varepsilon > 1$

Table 1. The conditions for rainbow trapping. $\sigma_\varepsilon = \left|\varepsilon_{\mathrm{II}} / \varepsilon_{\mathrm{I}}\right|$ and $\sigma_\mu = \left|\mu_{\mathrm{II}} / \mu_{\mathrm{I}}\right|$ where the subscripts I and II denote the core and the cladding respectively. For INI TE modes, replace $\sigma_\varepsilon \leftrightarrow \sigma_\mu$.

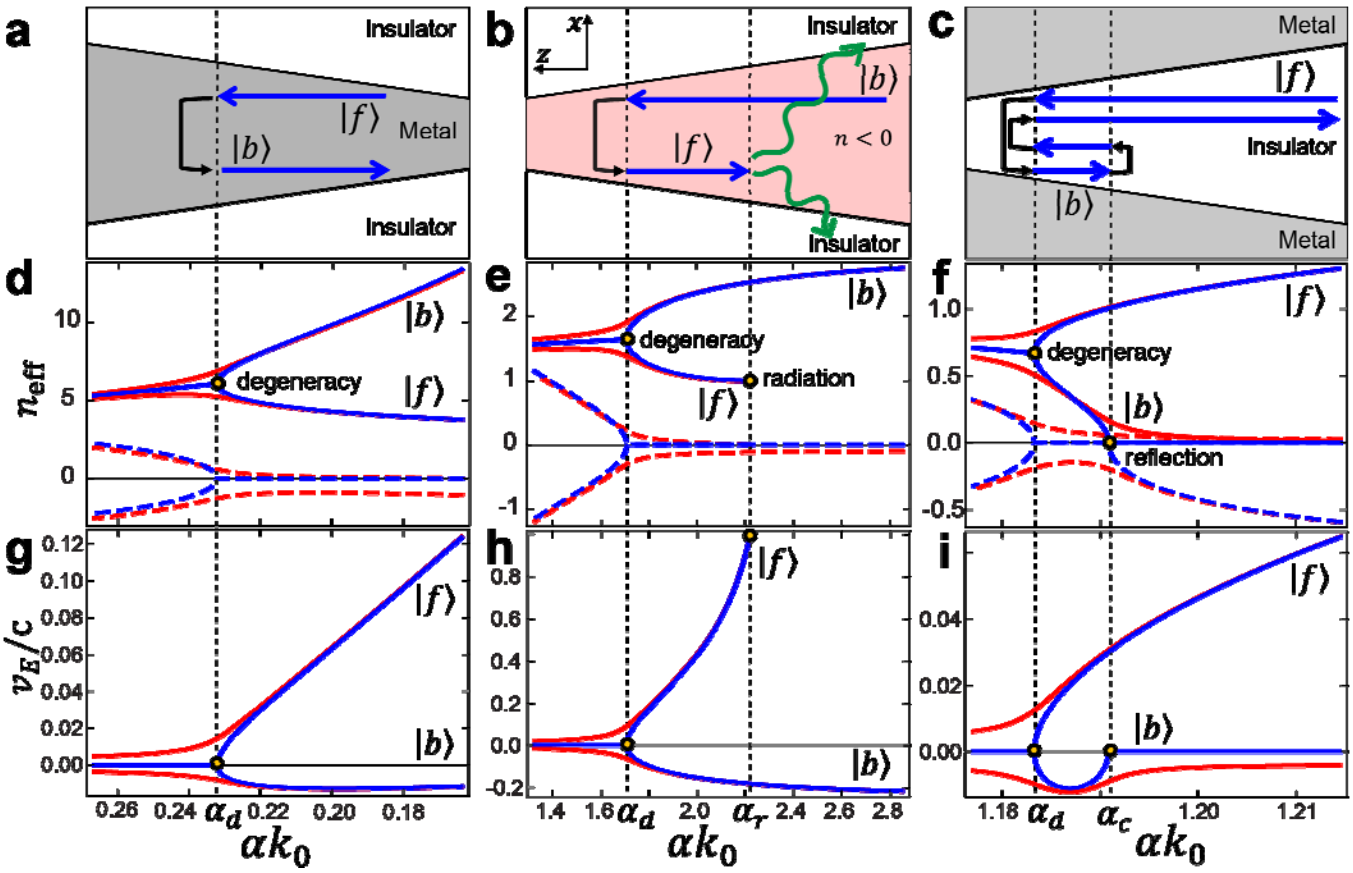

Figure 1. Schematic descriptions of (a)-(c) mode conversion mechanism, (d)-(f) n_{eff} and (g)-(i) v_E of IMI($\varepsilon_{\text{I}} = -8.5$, $\varepsilon_{\text{II}} = 10$) TM_0 , INI($\varepsilon_{\text{I}} = \mu_{\text{I}} = -3$, $\varepsilon_{\text{II}} = \mu_{\text{II}} = 1$) TM_2 , and MIM($\varepsilon_{\text{I}} = 10$, $\varepsilon_{\text{II}} = -1$) TM_2 modes versus αk_0 . In (d)-(f), real part and imaginary part of n_{eff} are represented as solid and dashed curves respectively. Lossless and lossy($\text{Im}\{\varepsilon\} / \text{Re}\{\varepsilon\} = 0.03$ for metal and $\text{Im}\{\varepsilon\} / \text{Re}\{\varepsilon\} = \text{Im}\{\mu\} / \text{Re}\{\mu\} = 0.03$ for negative index metamaterial) cases are plotted as blue and red curves respectively in (d)-(i). Dotted vertical lines indicate degeneracy point α_d , radiation point α_r , and the mode cutoff α_c .

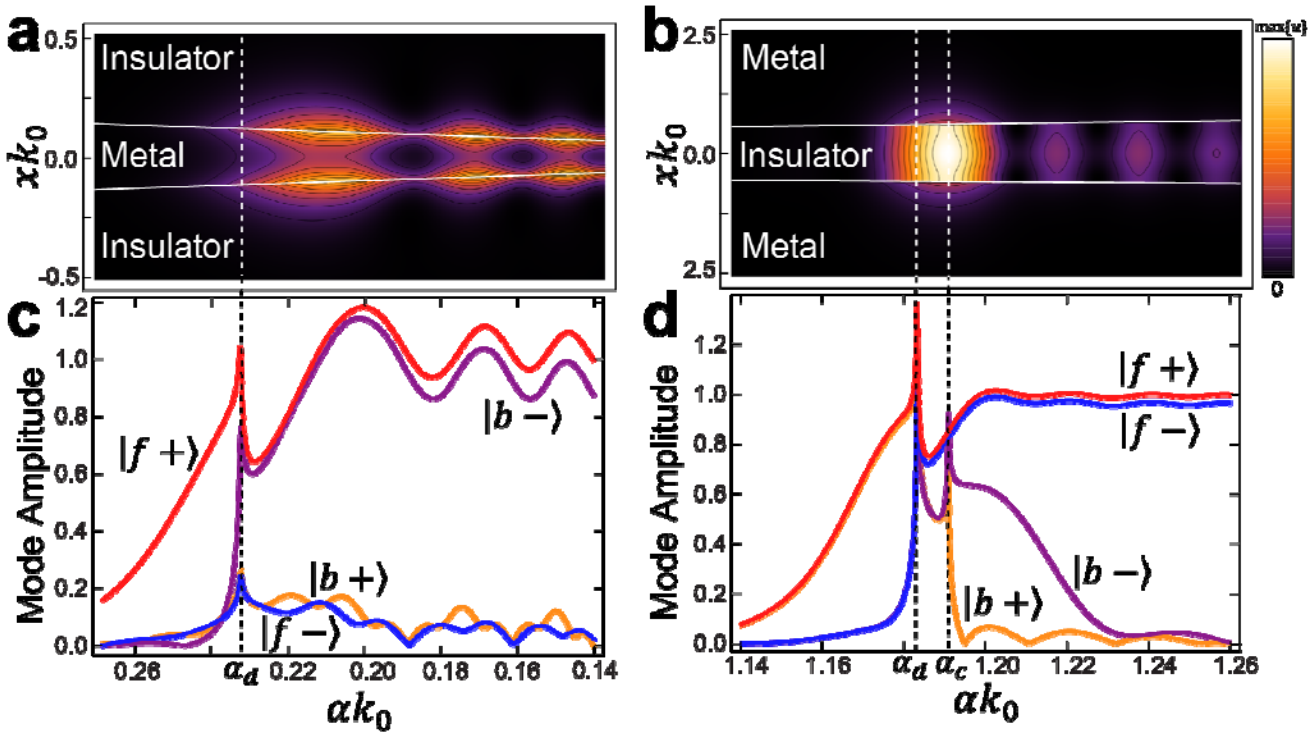

Figure 2. Energy density distribution $u(x,z)$ of (a) IMI ($\varepsilon_{\mathrm{I}}=-8.5$, $\varepsilon_{\mathrm{II}}=10+0.01i$) TM_0 and (b) MIM ($\varepsilon_{\mathrm{I}}=10$, $\varepsilon_{\mathrm{II}}=-1+0.001i$) TM_2 modes. Boundaries between core and claddings are indicated by white solid lines. (c),(d) Mode amplitudes of $|f+\rangle$ (red), $|f-\rangle$ (blue), $|b+\rangle$ (orange) and $|b-\rangle$ (purple) modes as functions of core thickness in the (c) IMI and (d) MIM structures. Dotted vertical lines indicate α_d and α_c.

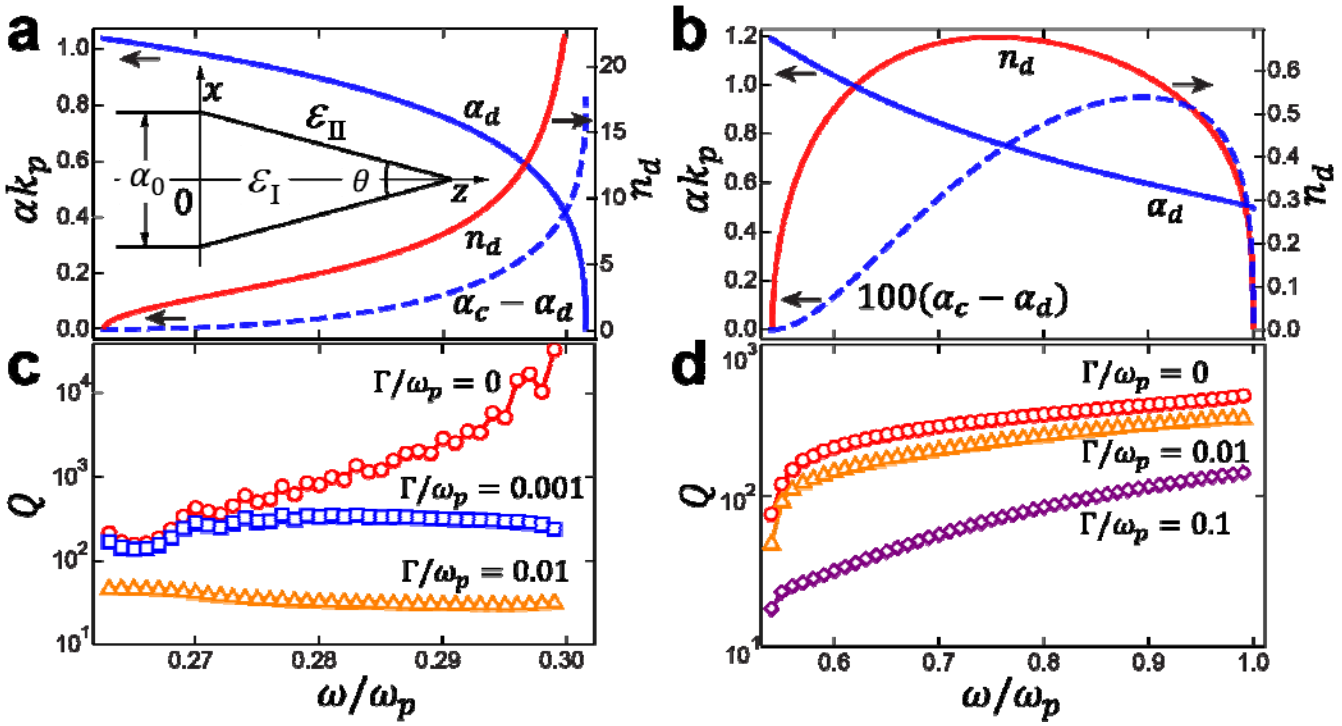

Figure 3. α_d (blue solid), $\alpha_c - \alpha_d$ (blue dashed, 100 times magnified in (b)) and n_d, the effective phase index of the mode at $\alpha = \alpha_d$ (red solid) of MIM ($\varepsilon_I = 10$, $\theta = 2^\circ$) (a) TM_1 and (b) TM_2 modes versus ω/ω_p. α_d and α_c are normalized by $k_p^{-1} = c/\omega_p$. The inset in (a) shows the schematic of a MIM rainbow trapping structure. Q versus ω/ω_p of (c) TM_1 modes for $\Gamma/\omega_p = \{0$ (red circles), 0.001(blue squares), 0.01(orange triangles)$\}$ and (d) TM_2 modes for $\Gamma/\omega_p = \{0$ (red circles), 0.01(orange triangles), 0.1(purple diamonds)$\}$.

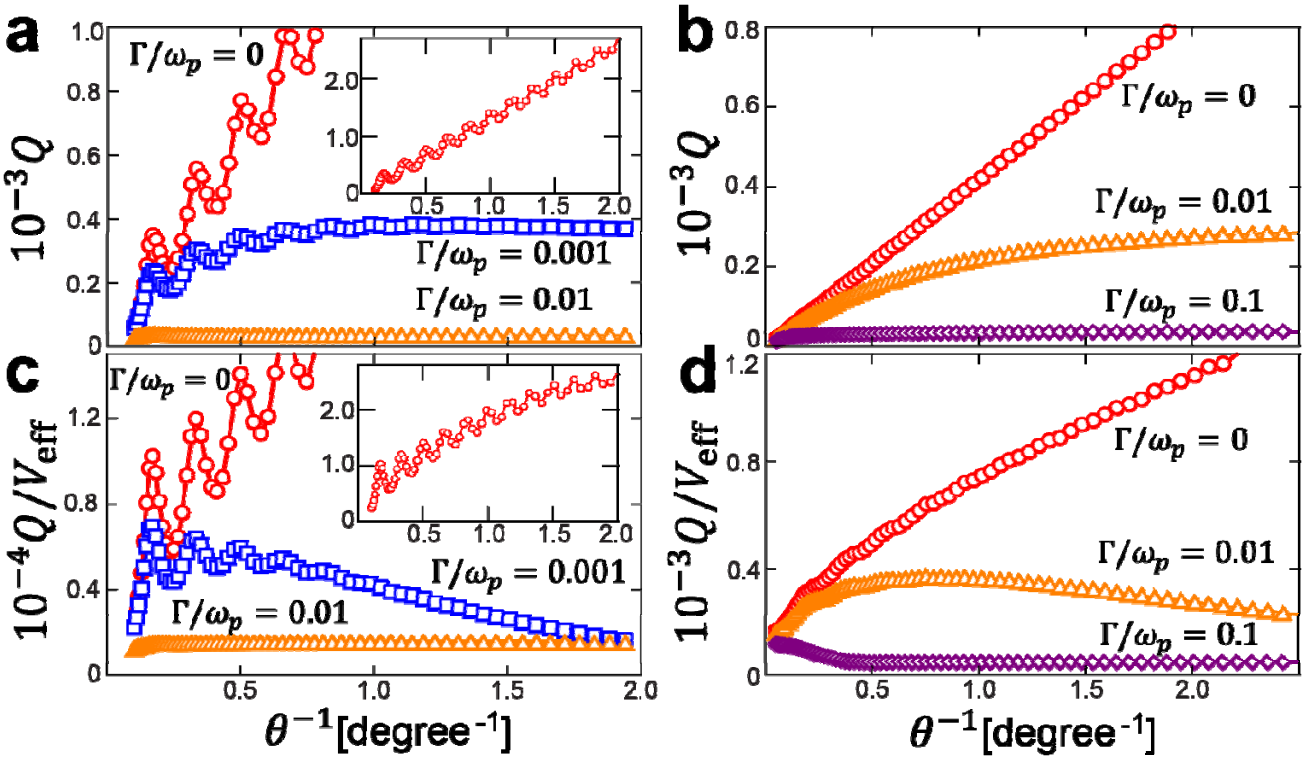

Figure 4. Q and Q/V_{eff} versus θ^{-1} of (a), (c) MIM ($\varepsilon_{\text{I}} = 10$) TM_1 modes at $\omega/\omega_p = 0.277$ for $\Gamma/\omega_p = \{0$ (red circles), 0.001(blue squares), 0.01(orange triangles)$\}$ and (b),(d) TM_2 modes at $\omega/\omega_p = 0.6$ for $\Gamma/\omega_p = \{0$ (red circles), 0.01(orange triangles), 0.1(purple diamonds)$\}$. The insets in (a) and (c) respectively plot Q and Q/V_{eff} for $\Gamma = 0$ in full range. Q/V_{eff} is normalized by $\left(\lambda_0/n_{\text{I}}\right)^{-3}$.